Supporting information (SI): New insight into the formation and aging processes of organic aerosols from positive matrix factorization analysis to ambient FIGAERO-CIMS thermograms

Section S1. Dataset separation and source apportionment for FIGAERO-OA

We first divided the dataset into 3 parts: part 1 (18690×1028), from 2 to 15 October; part 2 (18970×1028), from 16 to 30 October; part 3 (21840×1028), from 31 October to 16 November. In general, a significant change in Q/Q_{exp} was observed by increasing factors from 2 to 4 (Fig. S3). After investigating different solutions, an 8-factor solution was selected based on the performance of the Q/Q_{exp} values. The mass spectra of the 8 thermograms factors (referred as thermogrAMS-OA factors) of these three data sets can be found in Fig. S4. Since the entire campaign data set was divided into three parts, it is essential to perform the correlation analysis of mass spectra of 8 factors across different data sets (part 1 to 3) to identify the similar factors among the three data sets. In part 2 and 3 data sets, there were clear correlations between the respective factors, suggesting that the PMF results of part 2 and 3 data sets can be reasonably combined.

In part 1 data set, both factors 1 and 6 showed the highest correlation with factor 6 in the part 2 and 3 data set, respectively (fig. S5). However, there are no factors strongly correlated with F1 and F7 in part 2 and 3, respectively. It could be owing to that the sources of OA during 2 to 15 October (part 1) were different from those during 16 October to 16 November (part 2 and 3). In the discussion in sections 3.1 and 3.2, F1 and F7 in part 2 and 3 were believed to originate from photochemical reactions in the urban plumes and biomass burning, respectively. Figure S6 demonstrates that the site was mainly affected by south wind with a relatively lower concentration of BBOA and levoglucosan from 2 to 5 October. Thus, we performed PMF analysis to a new dataset (part 1.5), from 5 to 22 October. Clear correlations between the respective factors were found in part 1.5, 2, and 3 data sets (Fig. S5). Finally, we combined these three data sets (5 October to 16 November) in the manuscript.

Section S2. Estimation of oxidation state $\overline{OS_c}$ of organic compounds.

For non-nitrogen containing organic compounds, the $\overline{OS_C}$ can be estimated as:

$$\overline{OS_C} = 2 \times \frac{O}{C} - \frac{H}{C} \quad (1)$$

For nitrogen-containing organic compounds, the $\overline{OS_C}$ can be calculated from following equation:

$$\overline{OS_C} = 2 \times \frac{O}{C} - \frac{H}{C} - x \times \frac{N}{C} \quad (2)$$

where x is the valence state of N atoms, determined by functional groups. Here, several assumptions were adopted for classification. (1) nitrogen-containing functional groups were identified as nitro (-NO_2, x=+3) or nitrate (-NO_3, x=+5) in our measurement; (2) nitrogen-containing aromatics were assumed to contain nitro moieties, while nitrogen-containing aliphatic hydrocarbons were considered to contain nitrate moieties; (3) nitrogen-containing aromatics were characterized by having 6-9 carbon atoms and fewer hydrogen atoms compared to aliphatic hydrocarbons with the same number of carbon atoms.

Section S3. Description of ISORROPIA II model

Taking inorganic compounds (ammonium, sulfate, nitrate, and chloride) measured by the SP-AMS as input, A thermodynamic model ISORROPIA II was used to estimate aerosol liquid water content (ALWC) in this study. The model is run in "reverse" mode with the output chemical species in the metastable state. The effect of water-soluble organic compound, sodium, calcium, potassium, and magnesium was assumed to have minor impact on the ALWC in PM_1.

Table S1. Correlation between thermogram factors and AMS factors.

Experiment No.	Particle diameter (nm)	Mass loading (ng)	a	b
1	200	150.7	-0.197	1.056
2	200	241	-0.167	1.768
3	200	407	-0.206	3.732
4	100	90.5	-0.218	3.641
5	100	110.6	-0.241	5.229
6	100	150.8	-0.243	4.451

Table S2. Correlation between thermogram factors and AMS factors.

	MO-OOA	LO-OOA	BBSOA	HOA	BBOA	Night-OA
Day-HNO_x-LVOA	-0.06	0.70	0.35	-0.04	0.36	0.16
Day-LNO_x-LVOA	0.05	0.51	0.20	-0.04	0.32	-0.21
Day-aged-LVOA	0.13	0.78	0.50	-0.07	0.37	0.09
Day-aged-ELVOA	0.36	0.69	0.37	0.03	0.51	0.14
Day-urban-LVOA	0.15	0.70	0.28	0.01	0.31	0.40
Day-urban-ELVOA	0.27	0.73	0.34	0.05	0.44	0.32
BB-LVOA	-0.07	0.11	0.05	0.33	0.64	0.25
Night-LVOA	-0.18	0.37	0.40	0.15	0.29	0.49

Table S3. The detailed information of three selected periods.

	Periods	Days
Long-range Transport	14-20 October; 29-31 October; 3-4 November; 7-10 November; 14 November	17
Urban Air Masses	7-10 October; 23-27 October; 1-2 November;11 November; 13 November	13

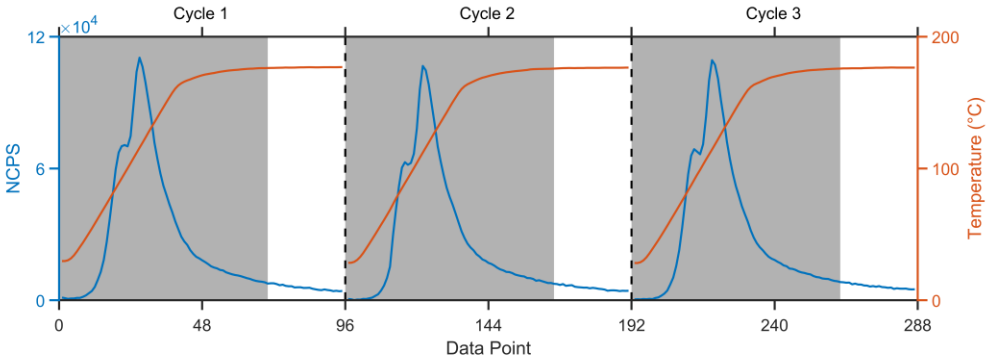

Figure S1. Example of measured total normalized count per second (NCPS) thermograms (blue line) and desorption temperature (red line) vs data points. The total NCPS is calculated based on total count per second (cps) of oxygenated organic compounds at all m/z (total cps), m/z 127 (cps_{127}), and m/z 145 (cps_{145}) measured by the FIGAERO-I-CIMS, $ncps = \frac{total\ cps}{(cps_{127}+cps_{145})\cdot 10^6}$. The gray area represents the input data points of PMF model.

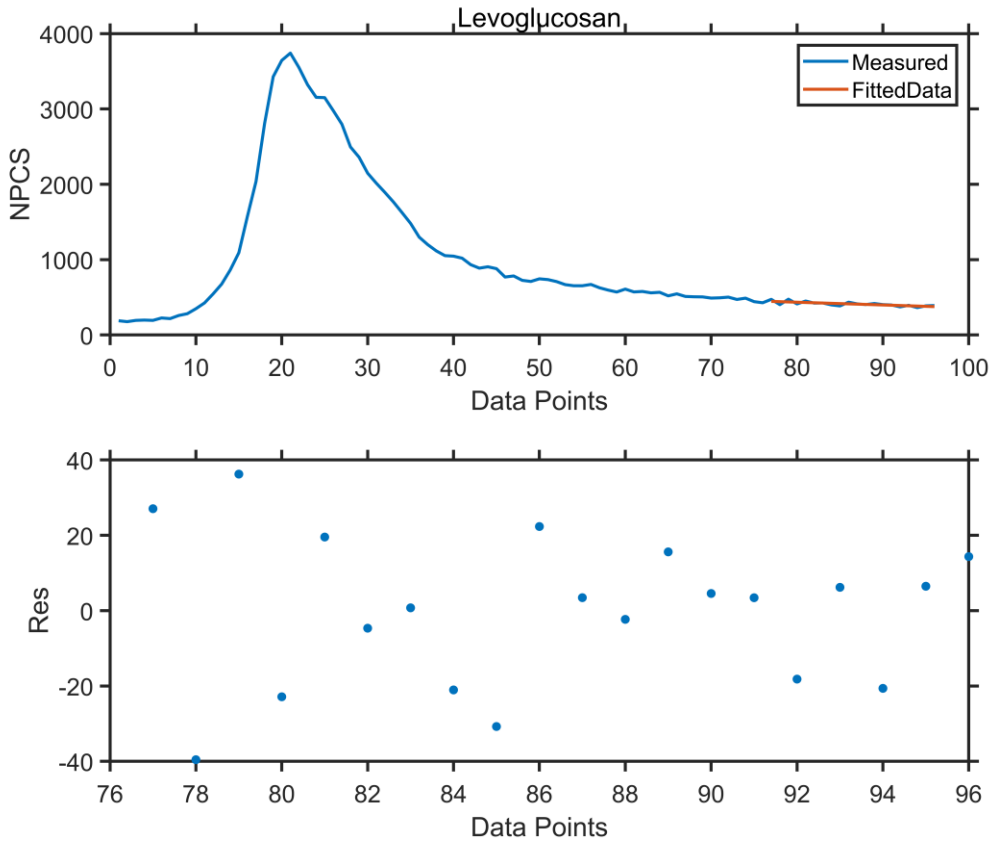

Figure S2. Example of measured NCPS, Fitted Data, and corresponding res_j of levoglucosan.

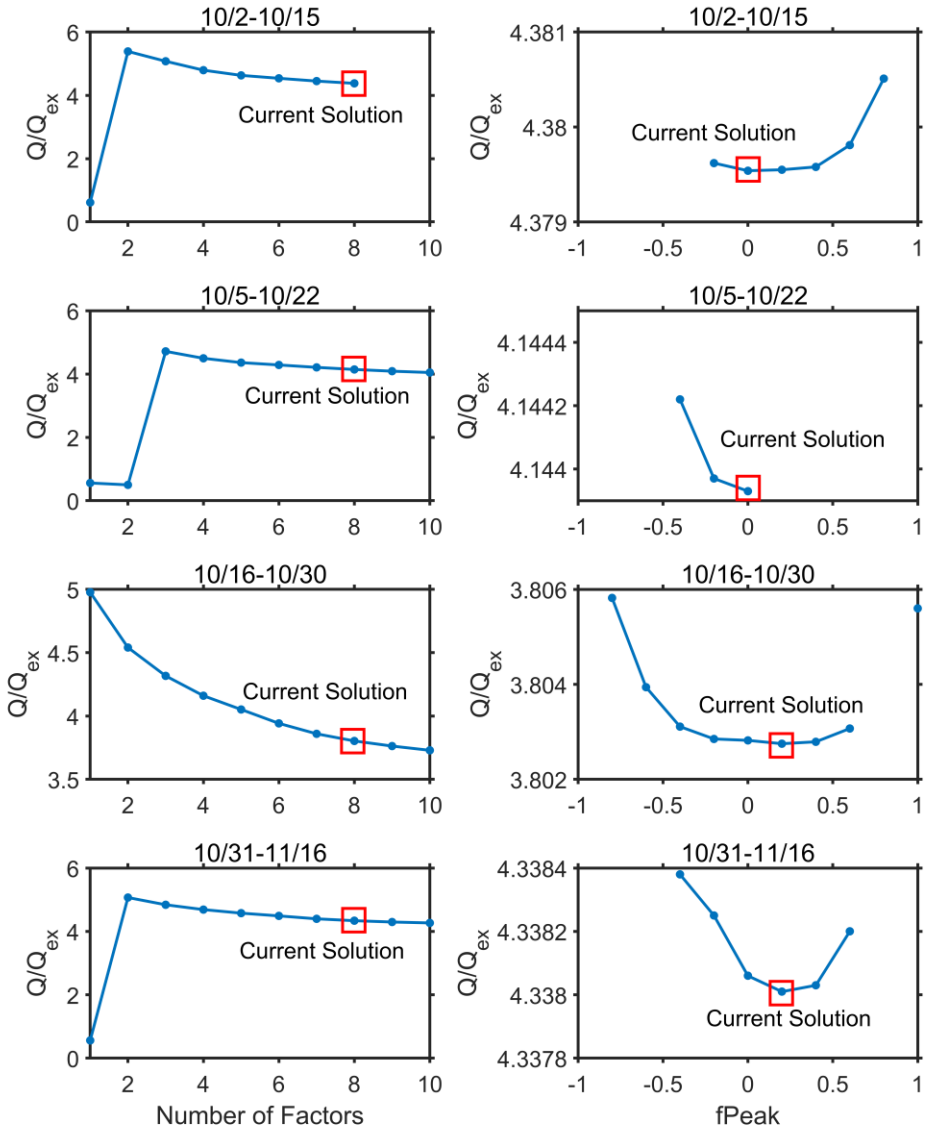

Figure S3. The Q/Q_{exp} values for part 1 (2 to 15 Oct.), part 1.5 (5 to 22 Oct.), part 2 (16 to 30 Oct.), and part 3 (31 Oct. to 16 Nov.).

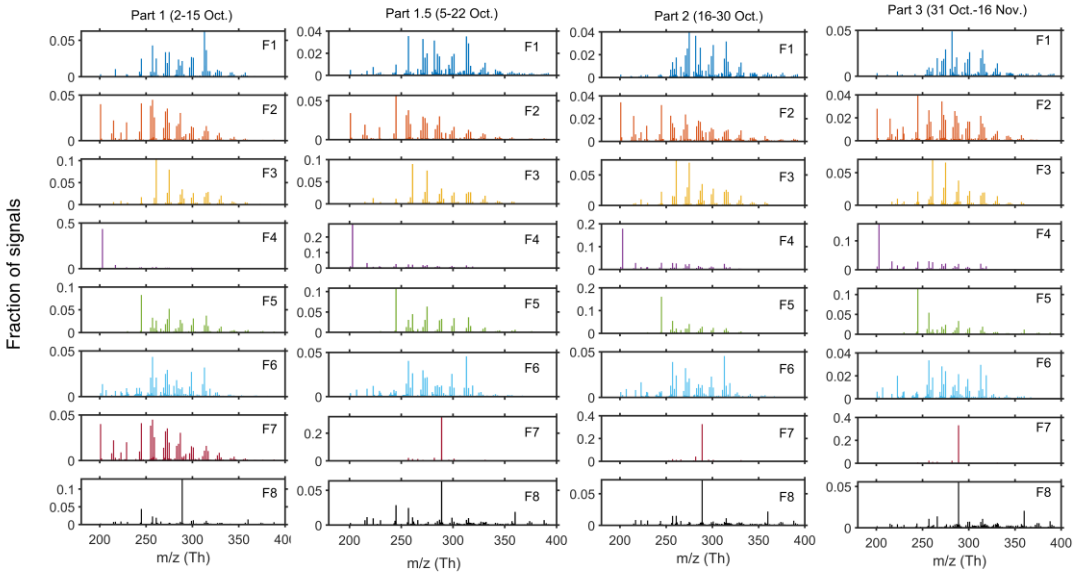

Figure S4. The mass spectra of 8 thermograms PMF factor of four data sets (part 1 to 3).

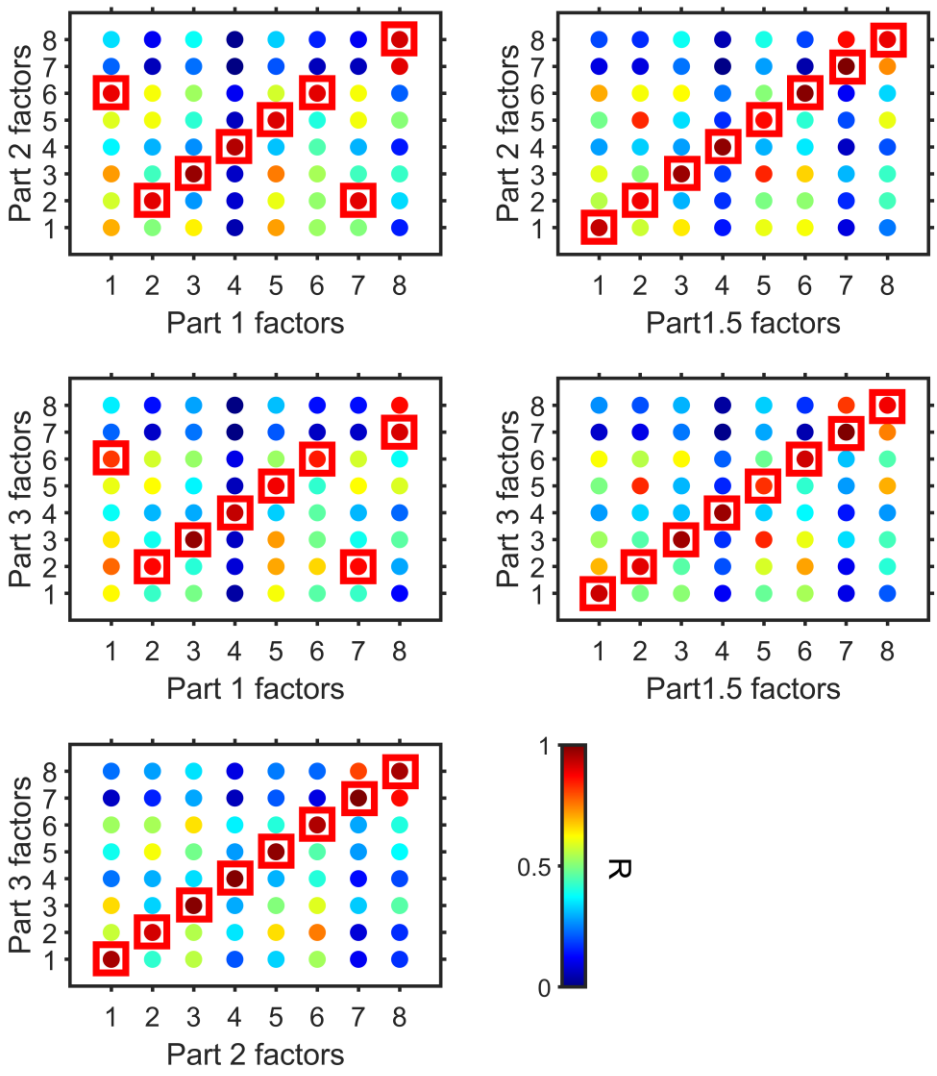

Figure S5. The correlation of mass spectra of 8 factors across different data sets (part 1 to 3). The red squares represent the highest R value for a specific factor along the x-axis compared to all factors on the y-axis.

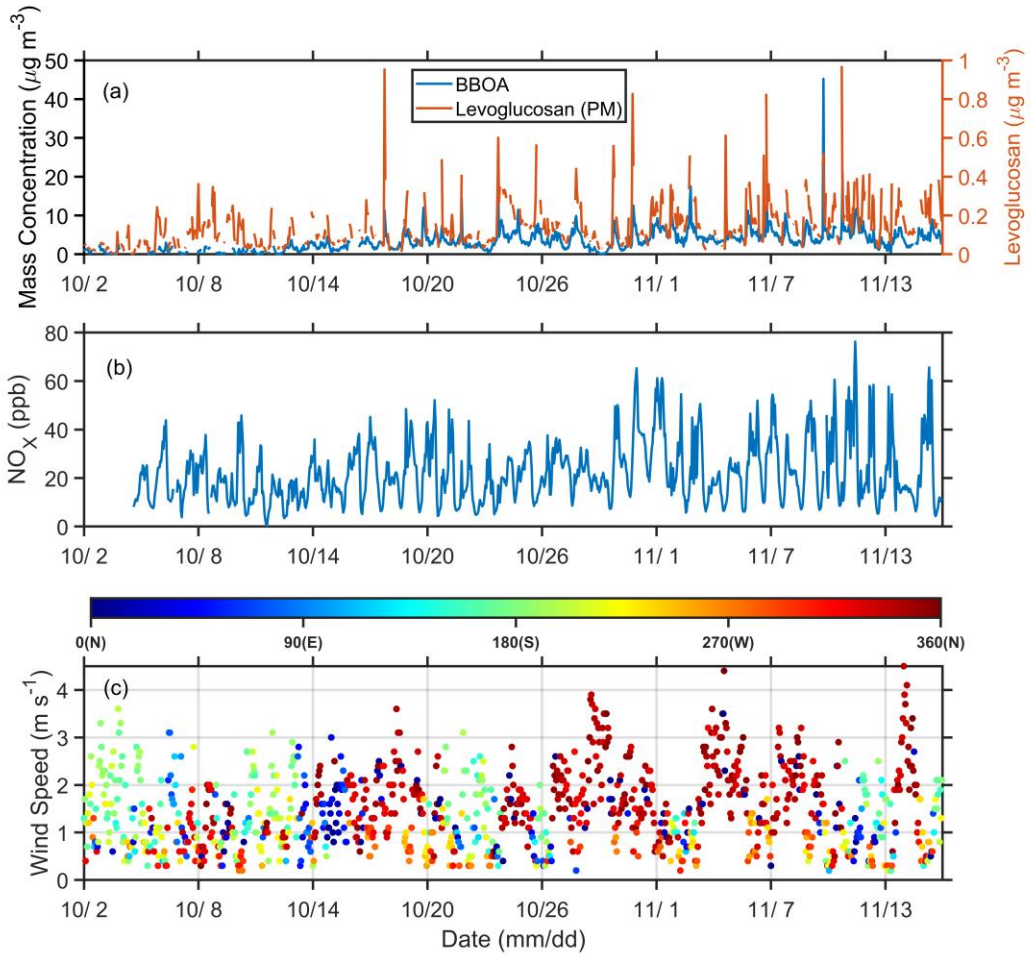

Figure S6. The timeseries of (a) levoglucosan in the particle phase measured by the FIGAERO-CIMS and BBOA in AMS-OA, (b) NO_x, and (c) wind speed and direction from 2 October and 16 November.

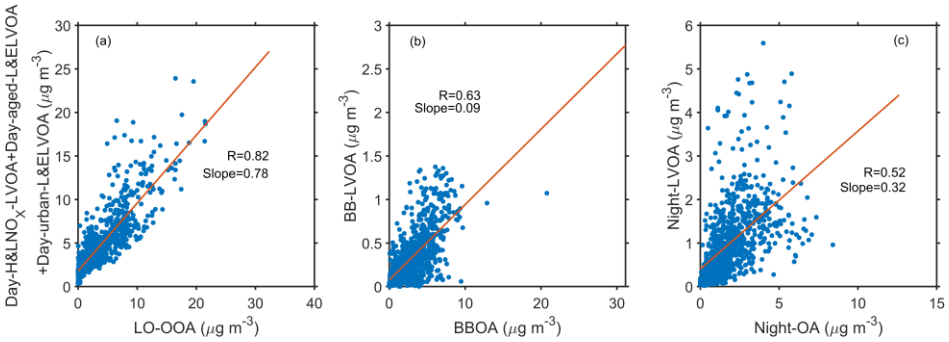

Figure S7. Correlation between FIGAERO-OA factors and AMS-OA factors.

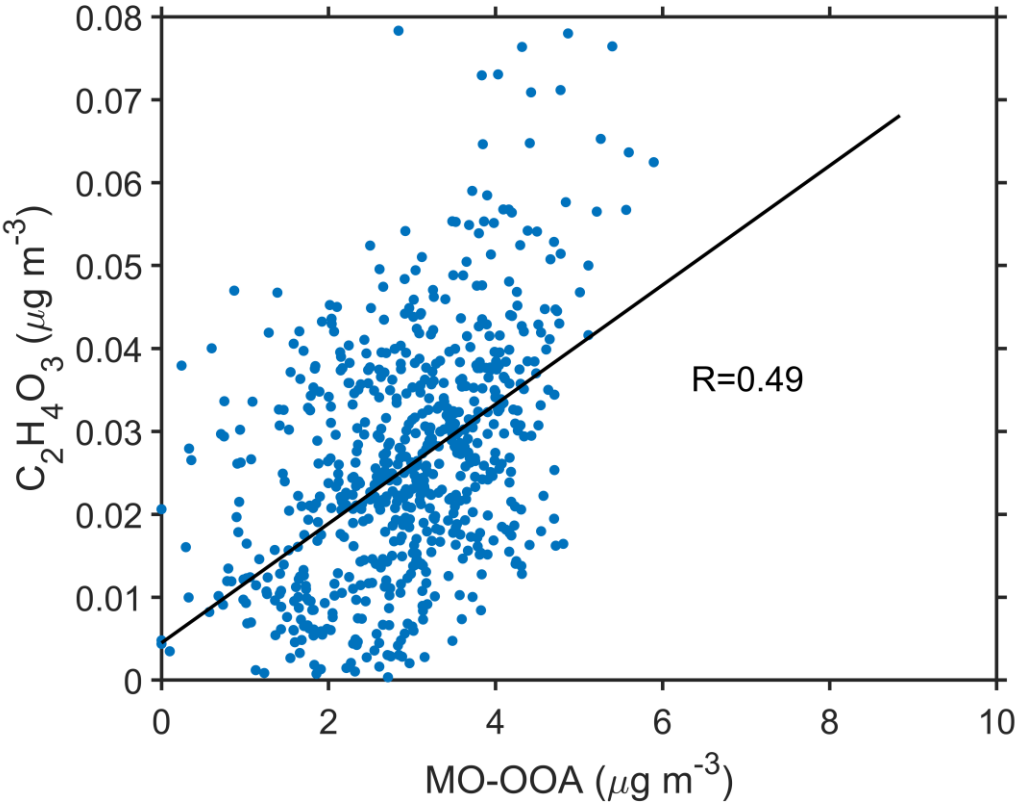

Figure S8. Correlation between $C_2H_4O_3$ and MO-OOA in AMS-OA.

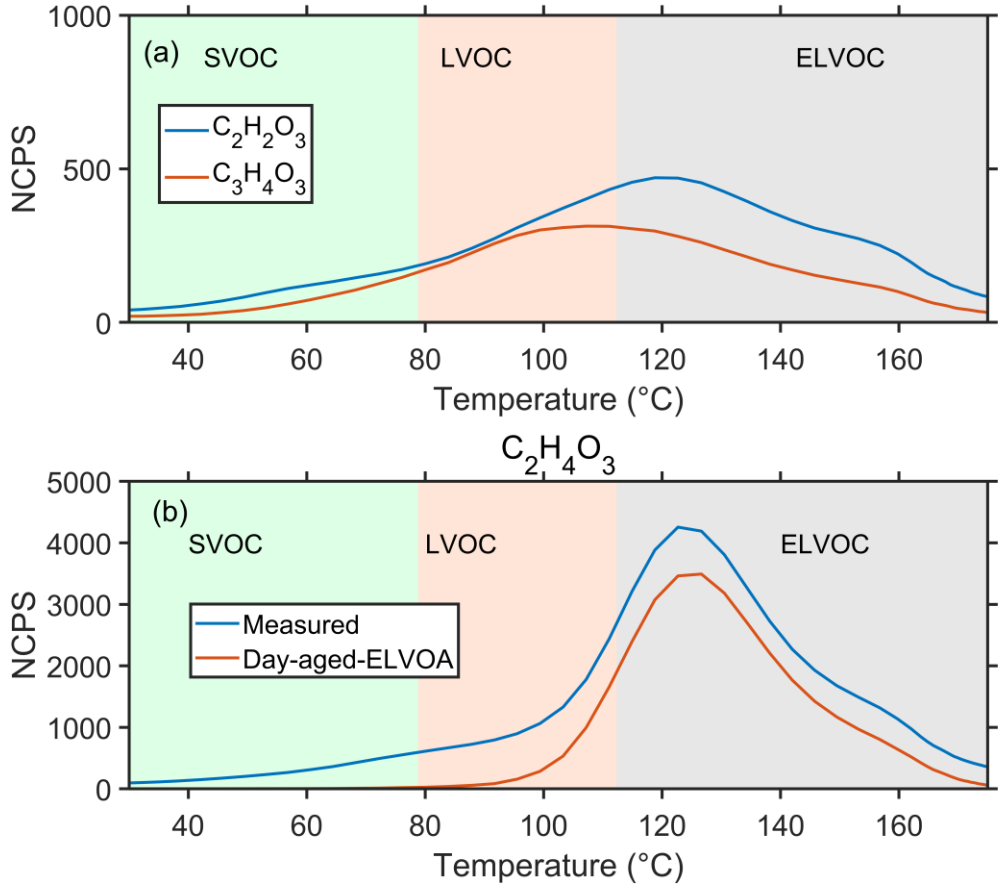

Figure S9. The average thermogram signals of (a) $C_2H_2O_3$, $C_3H_4O_3$, and (b) $C_2H_4O_3$. The blue line and red line in panel (b) represent the measured signal and the signal contributed by Day-aged-ELVOA, respectively.

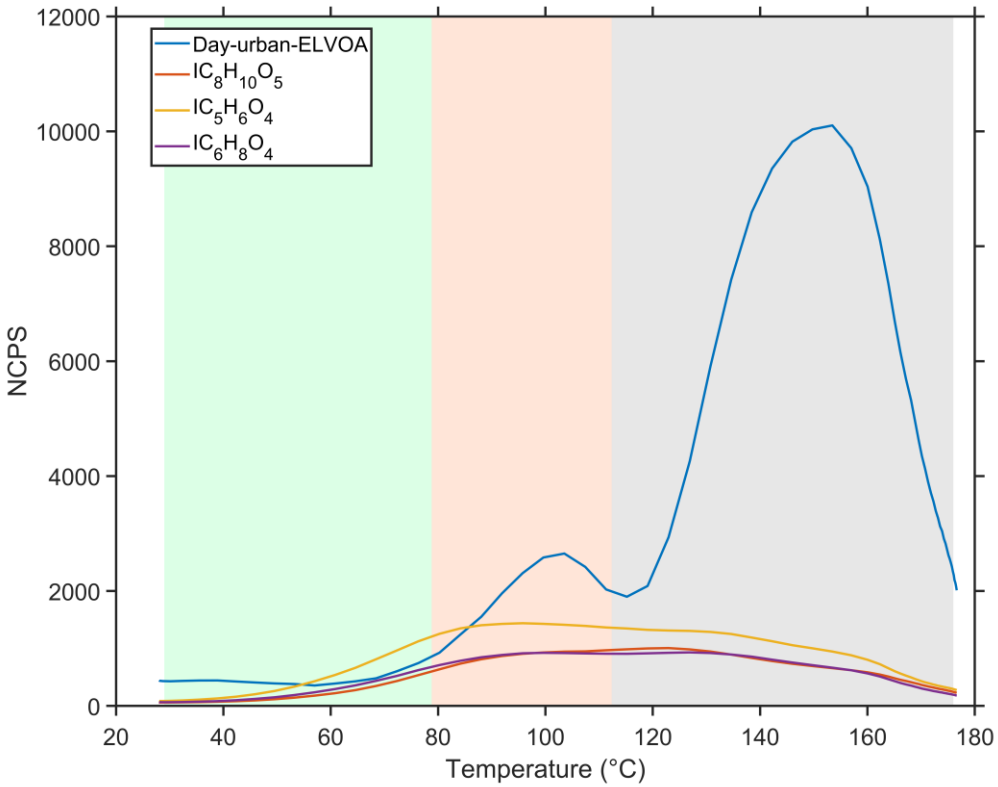

Figure S10. The average thermogram Day-urban-ELVOA, $C_8H_{10}O_5$, $C_5H_6O_4$, and $C_6H_8O_4$.

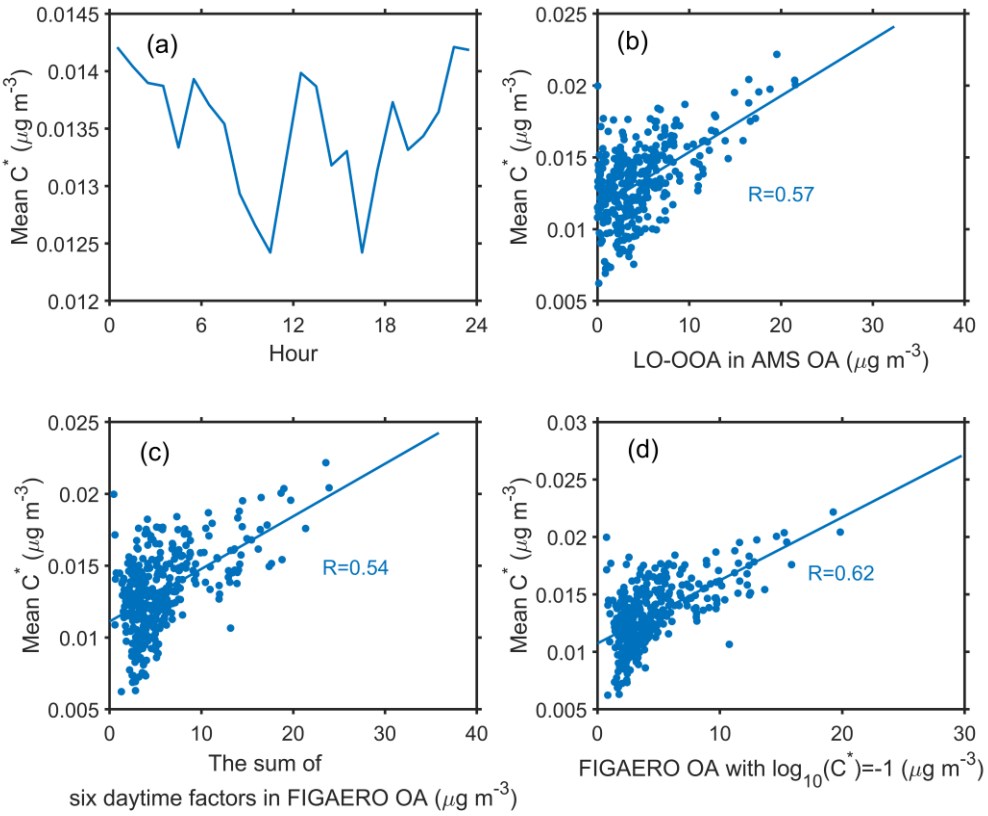

Figure S11. Diurnal variation of mean (a) C^* and scatter plot of mean C^* versus (b) LO-OOA from AMS, (c) the sum of six daytime factors (Day-HNO_x-LVOA, Day-LNO_x-LVOA, Day-aged-LVOA, Day-aged-ELVOA, Day-urban-LVOA, and Day-urban-ELVOA) in FIGAERO-OA, (d) FIGAERO-OA with a volatility at $\log_{10} C^*$=-1 during the daytime (6:00-18:00 LT).

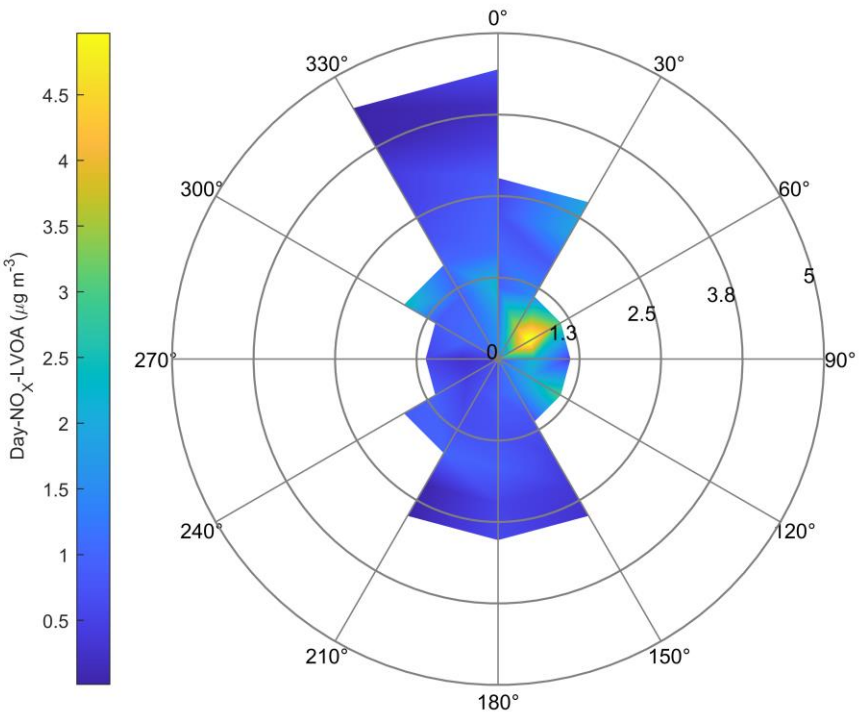

Figure S12. Rose plot of Day-HNO_x-LVOA under different wind direction and speed.

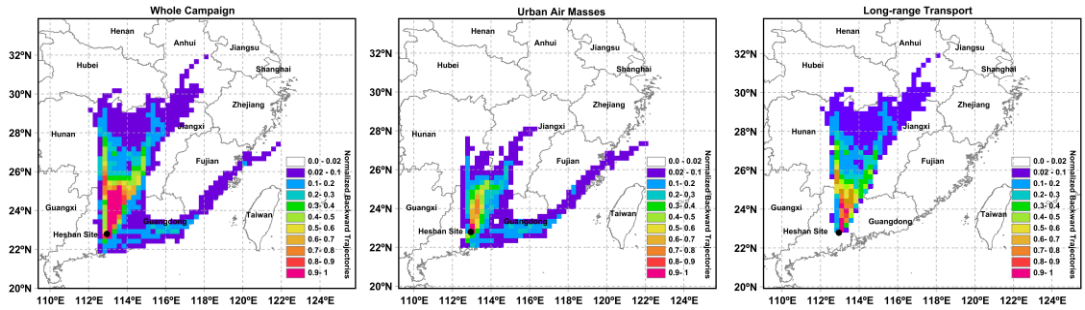

Figure S13. Normalized 72 hours backward trajectory analysis during the whole campaign, the urban air masses, and the long-range transport period

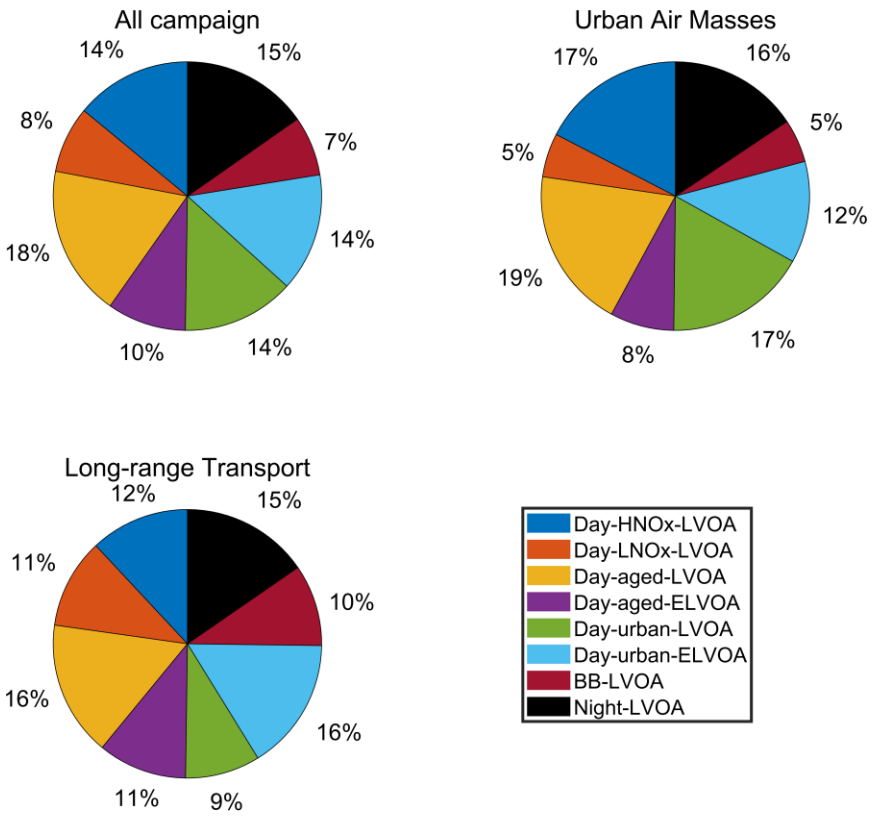

Figure S14. The average mass fraction of FIGAERO-OA during the whole campaign, the urban air masses and long-range transport period.

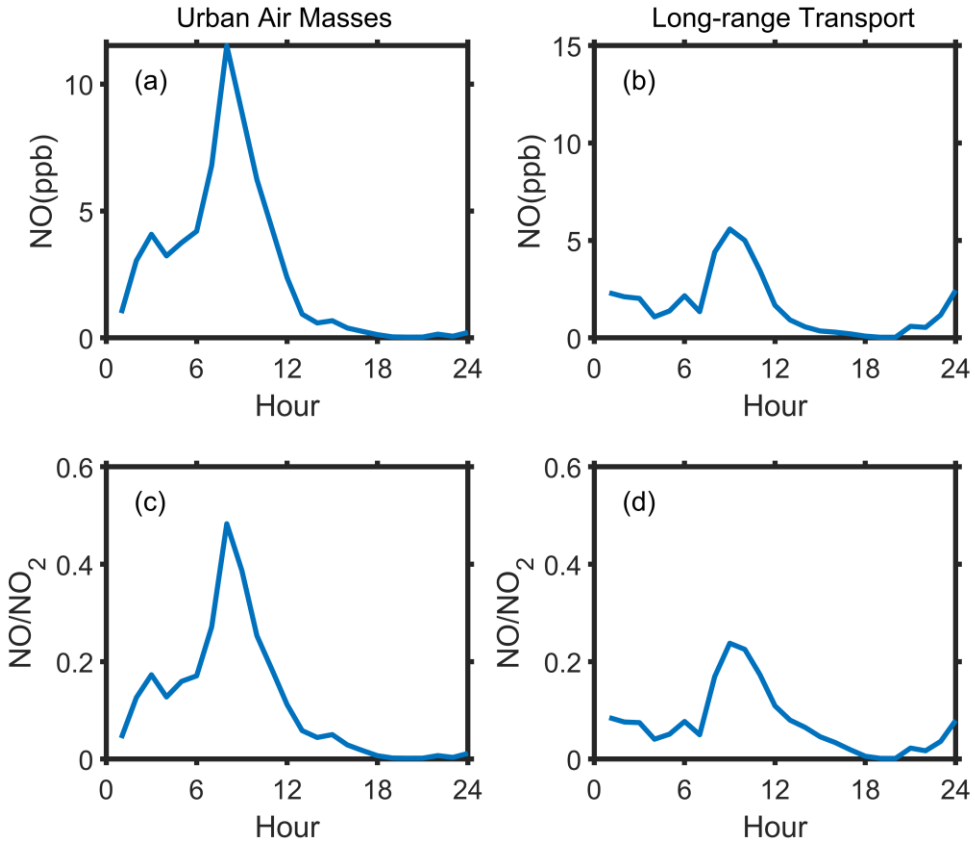

Figure S15. Average diurnal variation of NO and NO/NO_2 during the urban air masses and long-range transport period.

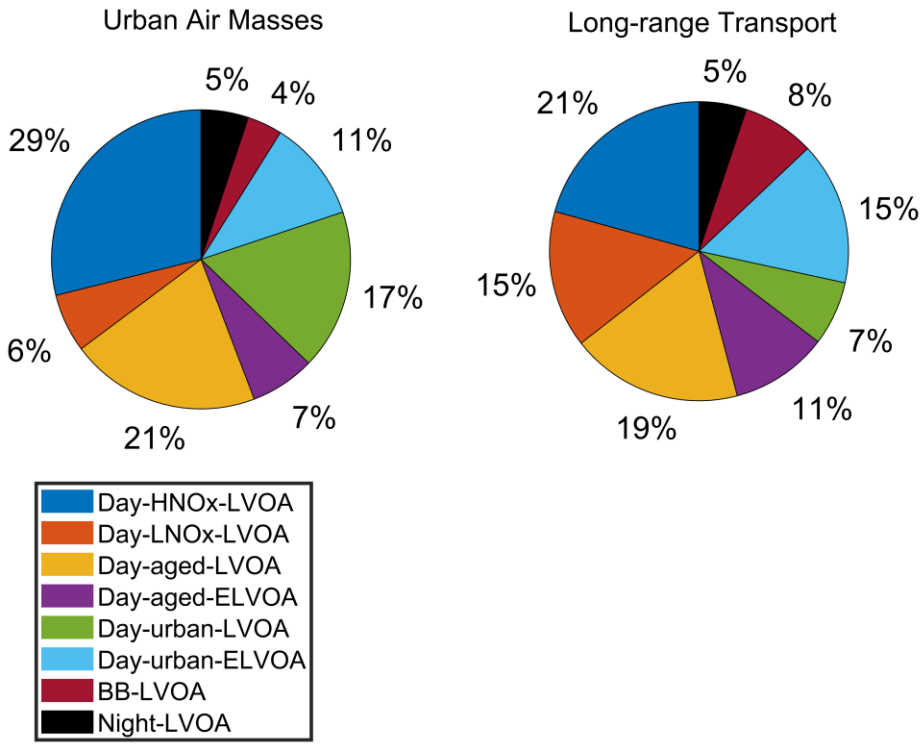

Figure S16. Pie charts of FIGAERO-OA in the afternoon (12:00-18:00 LT) during different periods.

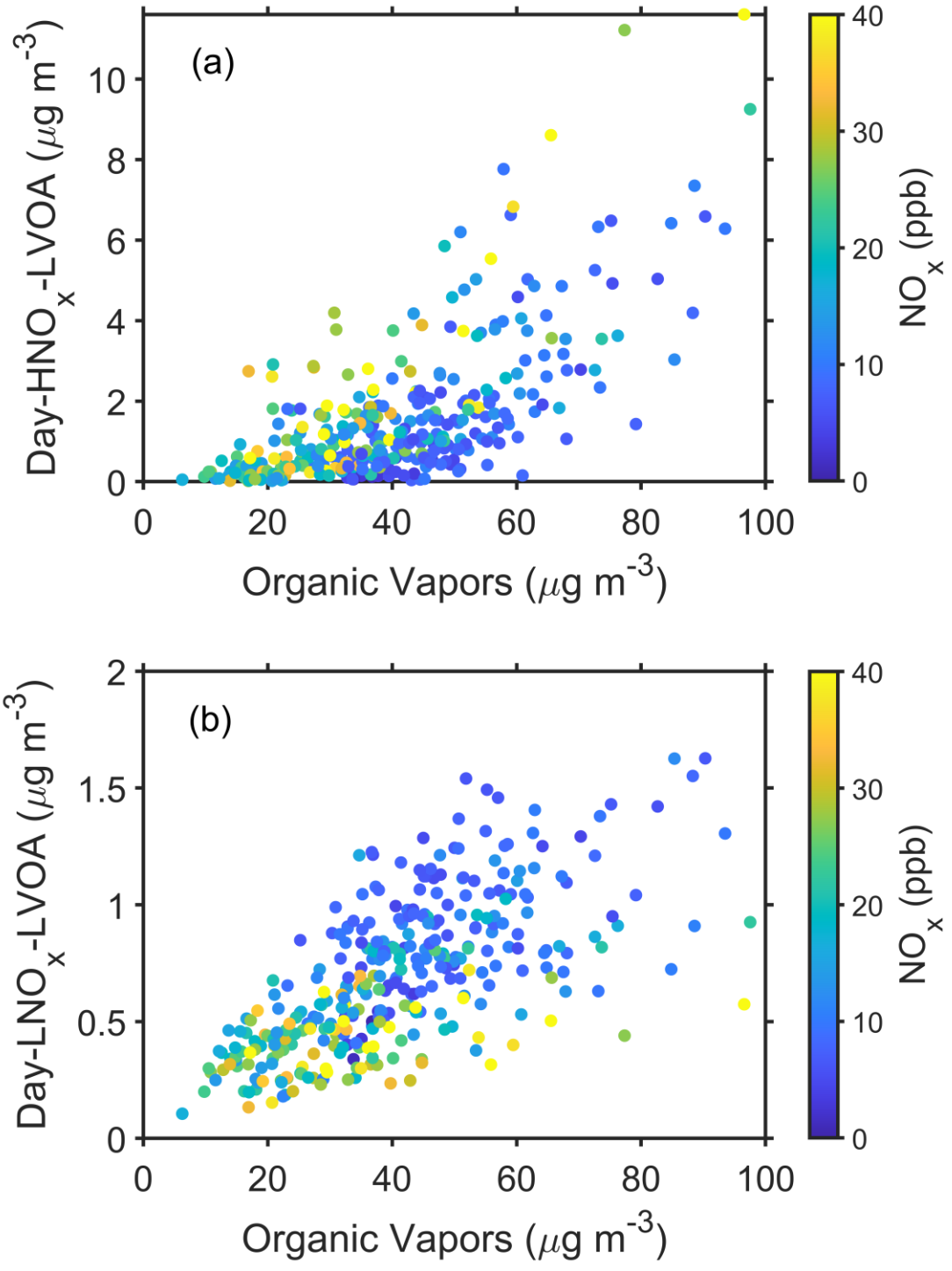

Figure S17. Scatter plot of Day-HNO$_x$-LVOA and Day-LNO$_x$-LVOA versus organic vapors under different NO$_x$ conditions.

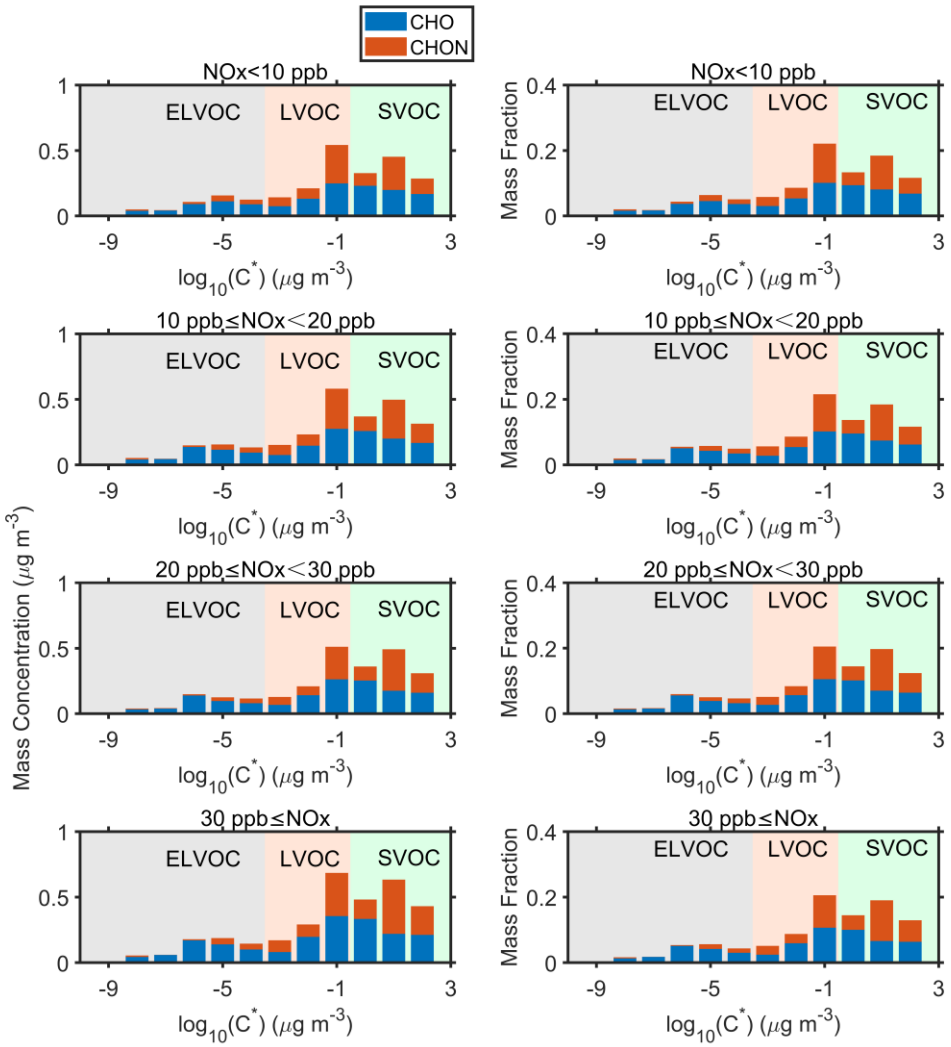

Figure S18. The average volatility distribution of non-nitrogen containing and nitrogen containing organic molecules in the gas phase under different NO_x levels at 12:00-16:00 LT. The estimation of volatility of gas-phase organic compounds is the same as Cai et al. (2024).

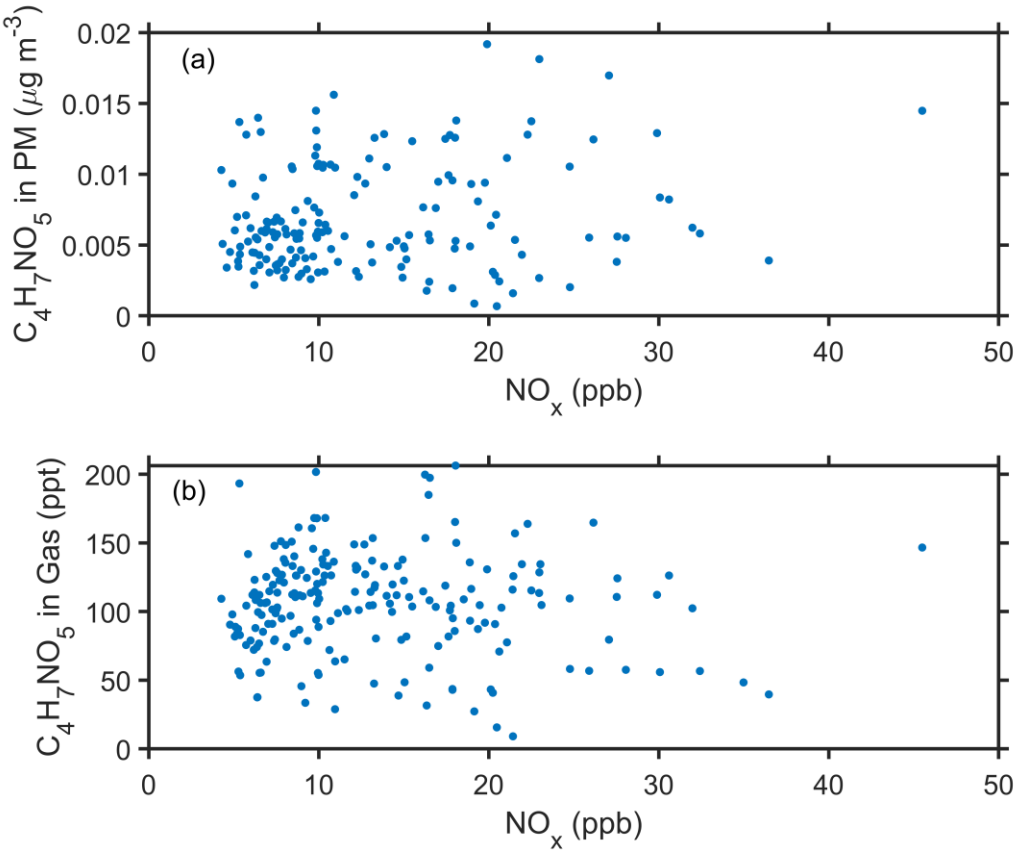

Figure S19. Relationship between $C_4H_7NO_5$ in particle- and gas-phase and NO_x.

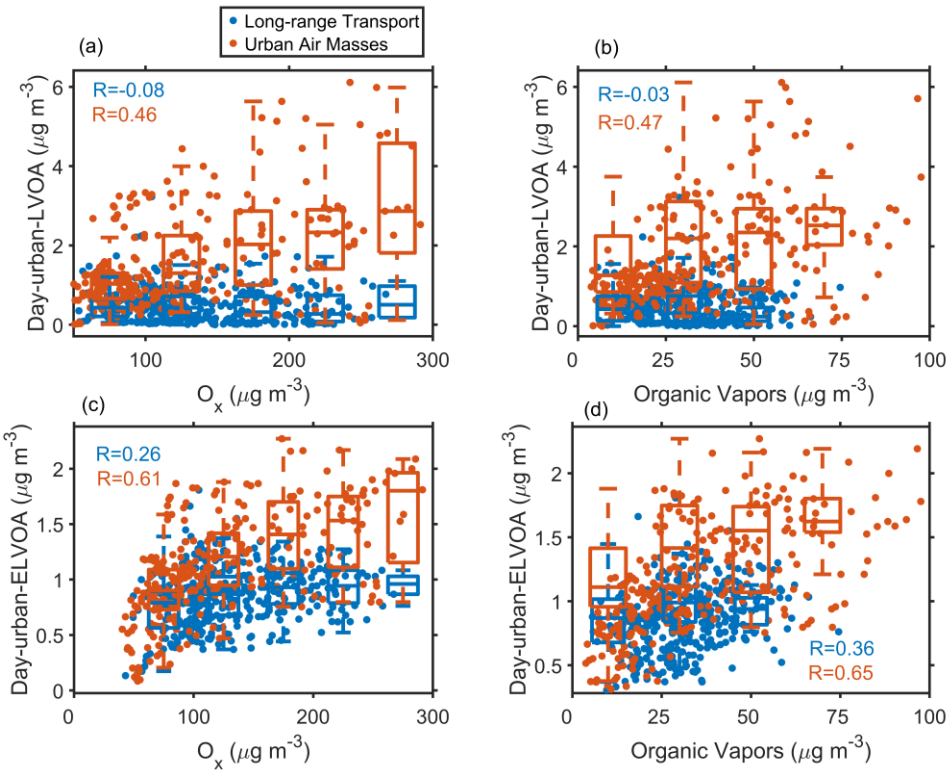

Figure S20. Variation of Day-urban-LVOA and Day-urban-ELVOA as a function of O_x and organic vapors during long-range transport period (blue) and urban air masses period (red).

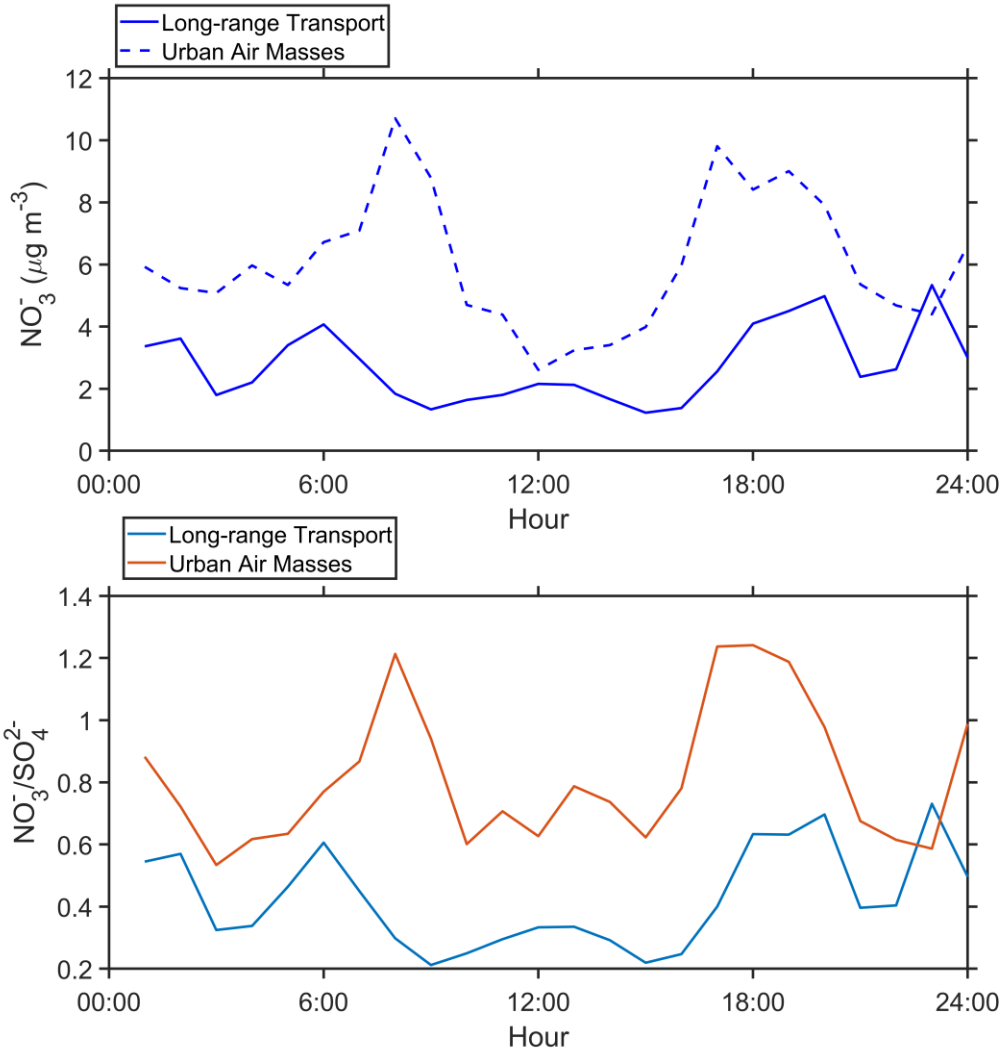

Figure S21. The average diurnal variation of nitrate and NO_3^-/SIA during the urban air masses and long-range transport period.

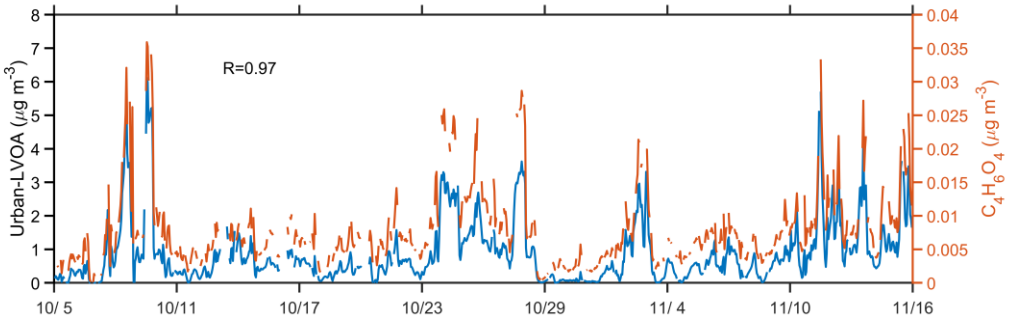

Figure S22. Timeseries of Day-urban-LVOA and $C_4H_6O_4$ in the particle phase.

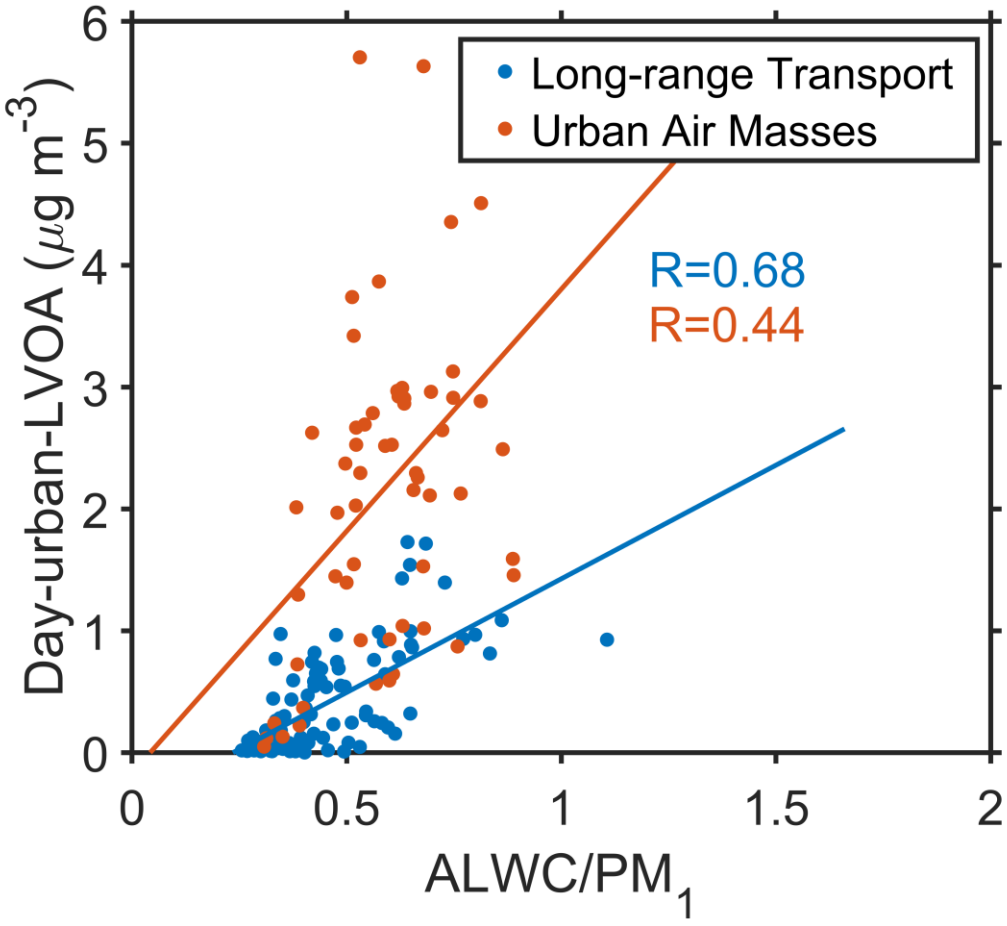

Figure S23. Relationship between Day-urban-LVOA and the ratio of aerosol liquid water content (ALWC) and PM_1. The estimation of ALWC was based on ISORROPIA II simulation. The description of ISORROPIA II can be found in section S3.

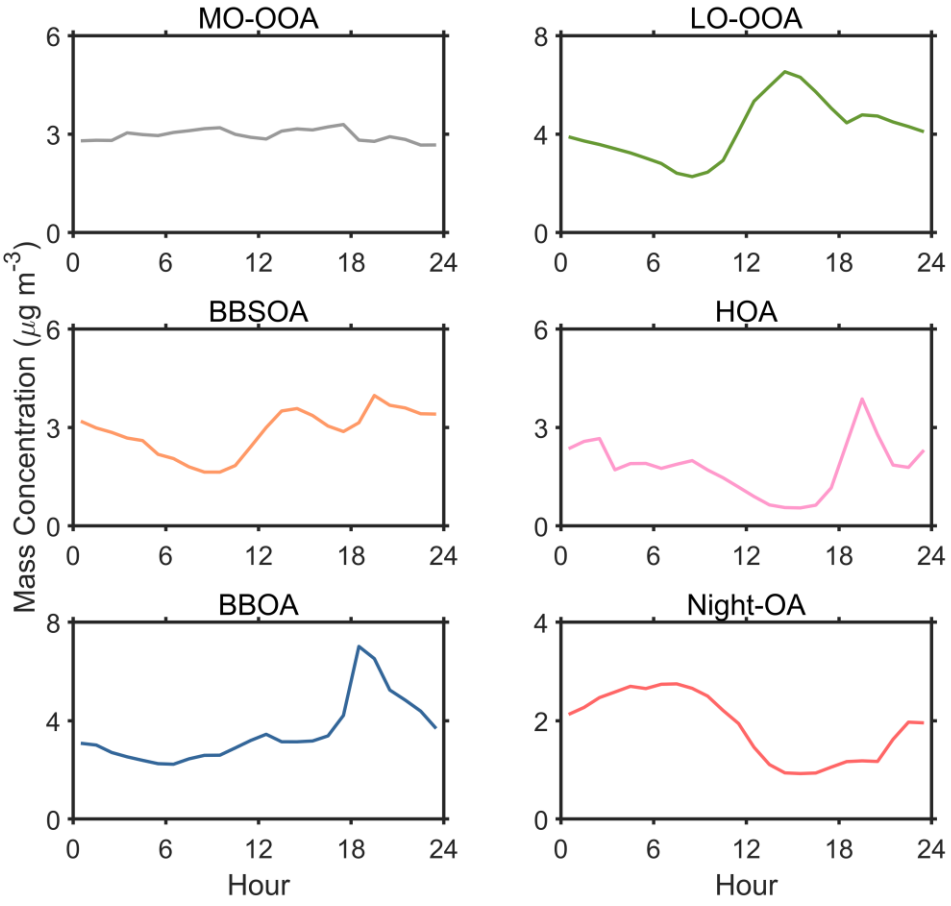

Figure S24. Diurnal variation of six PMF factors in AMS-OA.

Reference：

Cai, M., Ye, C., Yuan, B., Huang, S., Zheng, E., Yang, S., Wang, Z., Lin, Y., Li, T., Hu, W., Chen, W., Song, Q., Li, W., Peng, Y., Liang, B., Sun, Q., Zhao, J., Chen, D., Sun, J., Yang, Z., and Shao, M.: Enhanced daytime secondary aerosol formation driven by gas–particle partitioning in downwind urban plumes, Atmos. Chem. Phys., 24, 13065-13079, 10.5194/acp-24-13065-2024, 2024.